

Supplementary Materials for

Body-Wave Imaging of Earth's Mantle Discontinuities from Ambient Seismic Noise

P. Poli,* M. Campillo, H. Pedersen, LAPNET Working Group

*To whom correspondence should be addressed. E-mail: polip@ujf-grenoble.fr

Published 23 November 2012, *Science* **338**, 1063 (2012)
DOI: 10.1126/science.1228194

This PDF file includes:

Materials and Methods

Figs. S1 to S3

Table S1

References

Materials and Methods

Data processing

We calculated the noise correlation using data acquired during the year 2008 through the Polar Earth Observing Network (POLENET)/ Lapland Network (LAPNET) seismic array in northern Finland. Only the ZZ components were analyzed, in a frequency range from 0.1 Hz to 0.5 Hz. We first applied standard pre-processing: removal of the data mean and trend, prefiltering, resampling at an identical sampling rate (5 Hz), and deconvolution of the instrumental responses. Using earthquake data, the dataset had previously been through strict quality control to verify the instrument responses and correct for polarity problems.

We used the procedure of (22) to calculate the noise correlations. This procedure has been successful for the extraction of body waves in the crust at higher frequencies (22). We first split the continuous data into 4-h windows and removed those with amplitudes larger than three times the signal standard deviation, to suppress the effects of earthquakes and transitory instrument problems. The use of a short time window has been shown to increase the signal-to-noise ratio of the retrieved noise correlations (8, 22). For each remaining 4-h time window, we then applied spectral whitening in a frequency band from 0.1 Hz to 0.5 Hz, to diminish the dominance of waves related to the secondary microseismic peak at *ca.* 0.14 Hz.

We finally calculated the correlations of the 4-h time windows for each interstation pair and stacked these over the year. The resulting, folded, correlations are shown in Figure

S1, where all of the 861 correlations for the vertical-vertical components are plotted as a function of interstation distance.

Stacking

To enhance the body waves reflected from mantle discontinuities, we used techniques that are commonly applied in seismology (36) and in industrial applications that use active seismic surveys. This stack was composed of two steps. First, we used the AK135 standard Earth model (31) to align the correlations using the normal move-out velocity for P410P waves. As this normal move-out velocity is almost identical to the predicted normal move-out velocity for P660P waves, this procedure efficiently aligns the traces over the whole depth interval that we are interested in. We then muted the traces to times that corresponded to the surface wave arrivals, to avoid surface-wave contamination of the stack. Finally, we normalized each trace so that the peak amplitude was unity, and applied a slant stack (slowness ranging from -0.1 s/km to 0.1 s/km) to these muted, normalized correlations. Note that the P410P and P660P arrivals are expected to arrive at zero slowness, due to the normal move-out correction. The resulting slant stack is shown in Figure 1C.

Note that we applied the same stacking technique (including muting and normalization) to the correlations from the field data and to the synthetic seismograms.

Forward modeling

The synthetic seismograms were calculated by the discrete wavenumber integration method (37). We used a vertical force at the surface and calculated the earth displacement at the 861 distances that corresponded to our interstation distances for the field data.

For the comparison with the field data, we needed to have equivalent spectral content of the noise correlations and synthetics. We therefore whitened the spectra of the synthetic seismograms, and subsequently multiplied these spectra with the average amplitude spectrum of the correlations, which was evaluated around the theoretical arrival times of the P410P and P660P waves. We finally stacked the synthetic seismograms as explained in the previous section.

Ten models are explored here, with the parameterization showed in Table S1. The resulting zero-slowness traces for each parameterization are shown in Figure S3 (blue), and are compared with the stacked noise correlations (red).

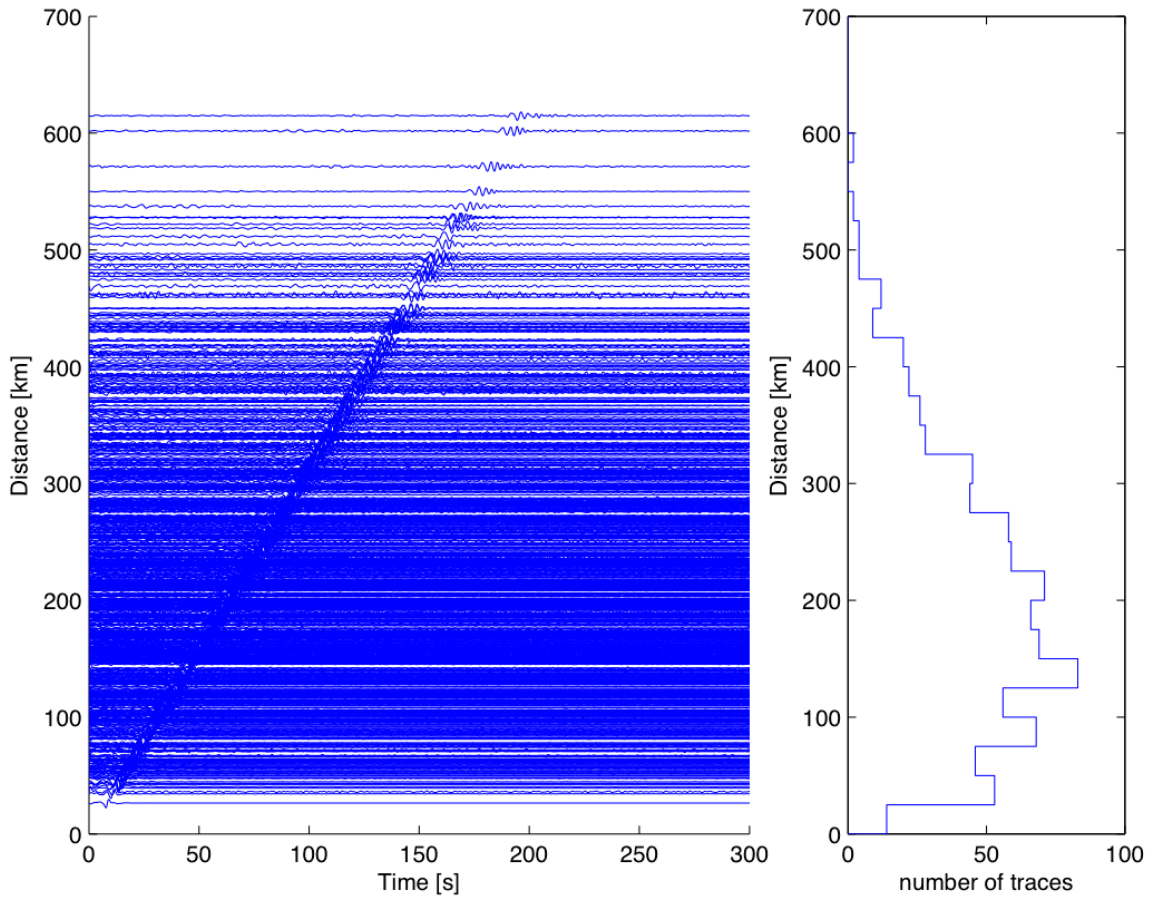


Fig. S1.

The 861 symmetrized noise correlations used in the present study. The frequency band spans from 0.1 Hz to 0.5 Hz. The noise correlations are dominated by Rayleigh waves. To extract small-amplitude body waves from the 410-km and 660-km discontinuities, we need to focus the analysis on time windows with no Rayleigh waves, and apply stacking techniques. The number of available traces for each 50-km distance is plotted on the right, to better illustrate the geometry of our array.

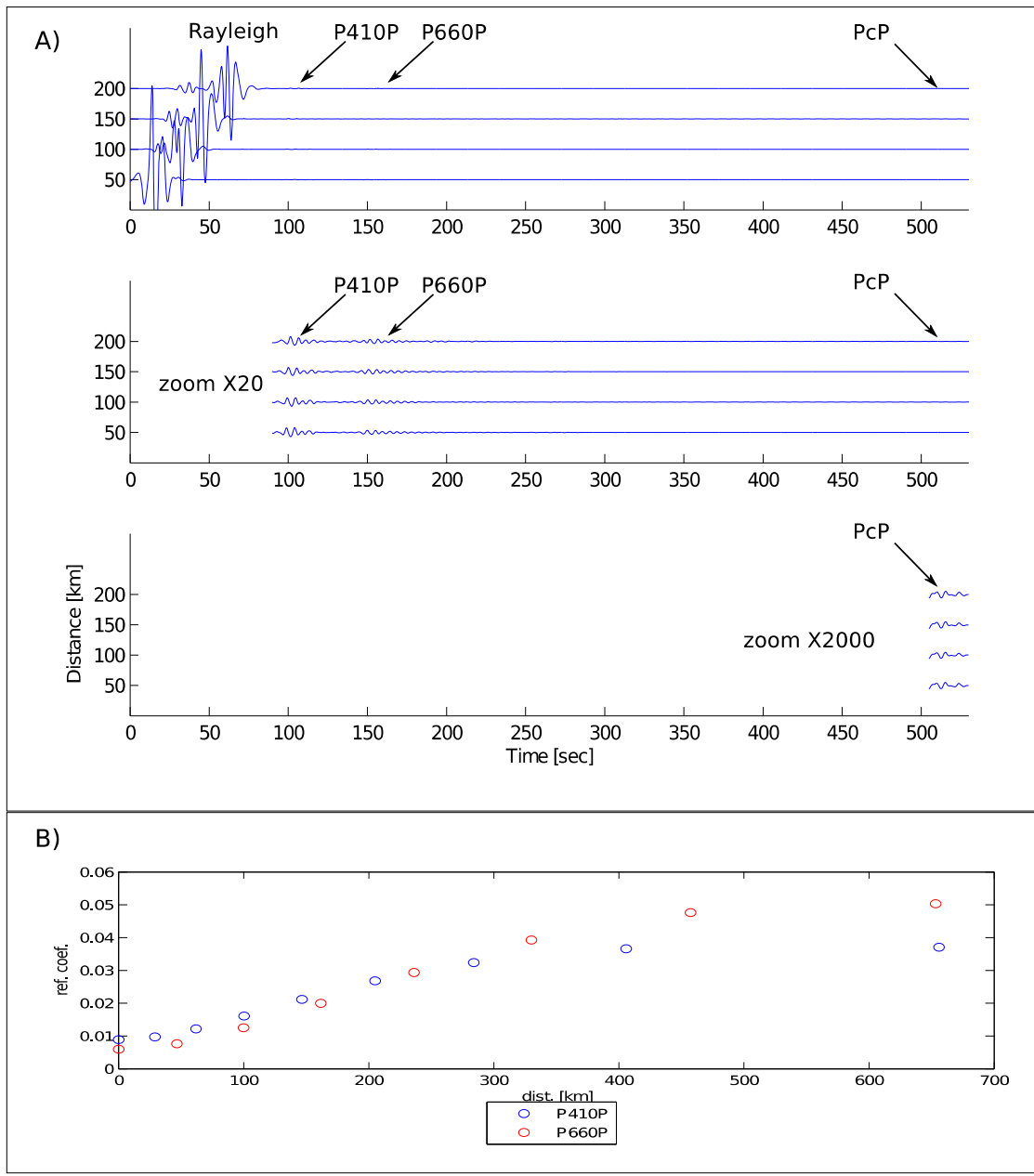


Fig. S2

A) Synthetic seismograms calculated using the Earth standard model AK135 are here plotted to show the difference in amplitude between the different phases. In this plot we focus on distances less than 200km where the surface waves and the other small amplitude body waves do not overlap in time.. The P660P and P410P have small amplitudes as compared to the surface waves, which is why they do not exceed the noise level in the correlations of field data for the individual station pairs. The P410P and P660P have amplitudes approximately fifty times higher than those of PcP, which possibly explains why these phases do not emerge even in the stacked correlations.

Figure S2-B shows the reflection coefficient for P4140P and P660P as predicted by AK135. Note that these coefficients do not account for geometrical spreading and anelastic attenuation.

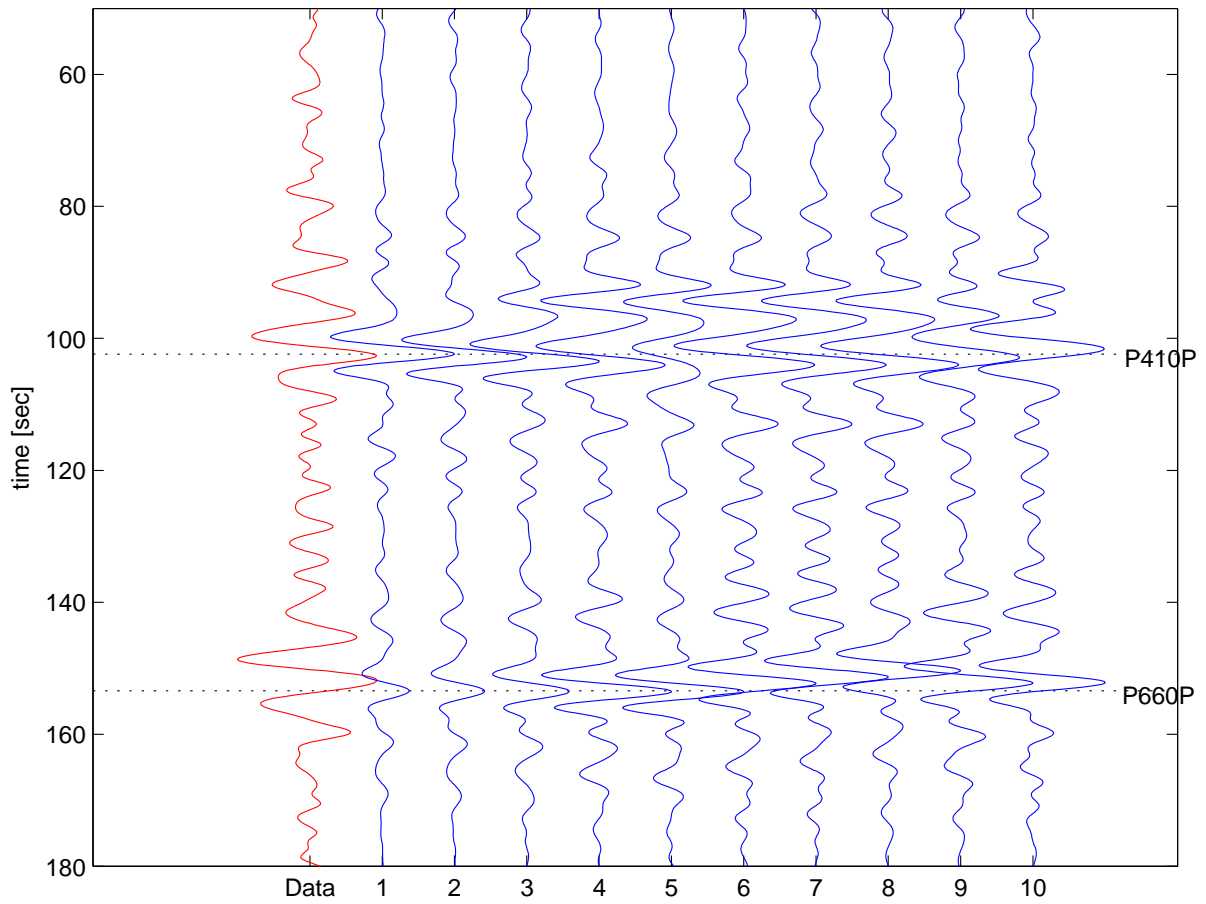


Fig. S3

Stack of the noise correlations calculated from the field data (red) and the synthetic seismograms (blue) that were generated using the models described in Table S1.

Model	'410' width	'410' depth	'660' width	'660' depth
	(km)	(km)	(km)	(km)
1 (AK135)	0	410	0	660
2	5	410	0	660
3	10	410	0	660
4	15	410	0	660
5	20	410	0	660
6	15	410	4	650
7	15	410	4	645
8	15	410	4	640
9	15	405	4	650
10	15	400	4	650

Table S1.

The models used to calculate the synthetic seismograms. All of the models were derived from the AK135 standard velocity model. The P-wave velocity increases linearly across the thickness of the discontinuities.

References

1. D. Zhao, Global tomographic image of mantle plumes and subducting slabs: Insight into deep Earth dynamics. *Phys. Earth Planet. Inter.* **146**, 3 (2004). [doi:10.1016/j.pepi.2003.07.032](https://doi.org/10.1016/j.pepi.2003.07.032)
2. C. Li, R. D. van der Hilst, E. R. Engdahl, S. Burdick, A new global model for P-wave speed variation in Earth's mantle. *Geochem. Geophys. Geosyst.* **9**, Q05018 (2008).
[doi:10.1029/2007GC001806](https://doi.org/10.1029/2007GC001806)
3. Q. Cao, R. D. van der Hilst, M. V. de Hoop, S. H. Shim, Seismic imaging of transition zone discontinuities suggests hot mantle west of Hawaii. *Science* **332**, 1068 (2011).
[doi:10.1126/science.1202731](https://doi.org/10.1126/science.1202731) [Medline](#)
4. Y. Gu, A. M. Dziewonski, C. B. Agee, Global de-correlation of the topography of transition zone discontinuities. *Earth Planet. Sci. Lett.* **157**, 57 (1998). [doi:10.1016/S0012-821X\(98\)00027-2](https://doi.org/10.1016/S0012-821X(98)00027-2)
5. P. Shearer, G. Masters, Global mapping of topography on the 660-km discontinuity. *Nature* **355**, 791 (1992). [doi:10.1038/355791a0](https://doi.org/10.1038/355791a0)
6. M. Campillo, A. Paul, Long-range correlations in the diffuse seismic coda. *Science* **299**, 547 (2003). [doi:10.1126/science.1078551](https://doi.org/10.1126/science.1078551) [Medline](#)
7. N. M. Shapiro, M. Campillo, Emergence of broadband Rayleigh waves from correlations of the ambient seismic noise. *Geophys. Res. Lett.* **31**, L07614 (2004).
[doi:10.1029/2004GL019491](https://doi.org/10.1029/2004GL019491)
8. G. A. Prieto, M. Denolle, J. F. Lawrence, G. C. Beroza, On the amplitude information carried by ambient seismic field. *C. R. Geosci.* **3**, 558 (2011).
9. N. M. Shapiro, M. Campillo, L. Stehly, M. H. Ritzwoller, High-resolution surface-wave tomography from ambient seismic noise. *Science* **307**, 1615 (2005).
[doi:10.1126/science.1108339](https://doi.org/10.1126/science.1108339) [Medline](#)
10. K. G. Sabra, P. Gerstoft, P. Roux, W. A. Kuperman, M. C. Fehler, Surface-wave tomography from microseisms in Southern California. *Geophys. Res. Lett.* **32**, L14311 (2005).
[doi:10.1029/2005GL023155](https://doi.org/10.1029/2005GL023155)

11. H. Yao, R. D. van der Hilst, Analysis of ambient noise energy distribution and phase velocity bias in ambient noise tomography, with application to SE Tibet. *Geophys. J. Int.* **179**, 1113 (2009). [doi:10.1111/j.1365-246X.2009.04329.x](https://doi.org/10.1111/j.1365-246X.2009.04329.x)
12. L. Stehly *et al.*, Tomography of the Alpine region from observations of seismic ambient noise. *Geophys. J. Int.* **178**, 338 (2009). [doi:10.1111/j.1365-246X.2009.04132.x](https://doi.org/10.1111/j.1365-246X.2009.04132.x)
13. F. C. Lin, M. H. Ritzwoller, R. Snieder, Eikonal tomography: Surface-wave tomography by phase-front tracking across a regional broad-band seismic array. *Geophys. J. Int.* **177**, 1091 (2009). [doi:10.1111/j.1365-246X.2009.04105.x](https://doi.org/10.1111/j.1365-246X.2009.04105.x)
14. M. S. Longuet-Higgins, A theory of the origin of microseisms. *Philos. Trans. R. Soc. London. Ser. A* **243**, 1 (1950). [doi:10.1098/rsta.1950.0012](https://doi.org/10.1098/rsta.1950.0012)
15. A. Friedrich, F. Krüger, K. Klinge, Ocean-generated microseismic noise located with the Gräfenberg array. *J. Seismol.* **2**, 47 (1998). [doi:10.1023/A:1009788904007](https://doi.org/10.1023/A:1009788904007)
16. N. Kobayashi, K. Nishida, Continuous excitation of planetary free oscillations by atmospheric disturbances. *Nature* **395**, 357 (1998). [doi:10.1038/26427](https://doi.org/10.1038/26427)
17. G. Ekström, Time domain analysis of Earth's long-period background seismic radiation. *J. Geophys. Res.* **106**, 26483 (2001). [doi:10.1029/2000JB000086](https://doi.org/10.1029/2000JB000086)
18. J. Rhie, B. Romanowicz, Excitation of Earth's continuous free oscillations by atmosphere-ocean-seafloor coupling. *Nature* **431**, 552 (2004). [doi:10.1038/nature02942](https://doi.org/10.1038/nature02942) [Medline](#)
19. G. Hillers *et al.*, Global oceanic microseism sources as seen by seismic arrays and predicted by wave action models. *Geochem. Geophys. Geosyst.* **13**, Q01021 (2012). [doi:10.1029/2011GC003875](https://doi.org/10.1029/2011GC003875)
20. Z. Zhan, S. Ni, D. V. Helmberger, R. W. Clayton, Retrieval of Moho-reflected shear-wave arrivals from ambient seismic noise. *Geophys. J. Int.* **182**, 408 (2010).
21. E. Ruigrok, X. Campman, K. Wapenaar, Extraction of P-wave reflections from microseisms. *C. R. Geosci.* **343**, 512 (2011). [doi:10.1016/j.crte.2011.02.006](https://doi.org/10.1016/j.crte.2011.02.006)
22. P. Poli, H. A. Pedersen, M. Campillo, POLENET/ LAPNET Working Group, Emergence of body waves from cross-correlation of seismic noise. *Geophys. J. Int.* **188**, 549 (2012). [doi:10.1111/j.1365-246X.2011.05271.x](https://doi.org/10.1111/j.1365-246X.2011.05271.x)

23. P. Roux, P-waves from cross-correlation of seismic noise. *Geophys. Res. Lett.* **32**, L19303 (2005). [doi:10.1029/2005GL023803](https://doi.org/10.1029/2005GL023803)
24. P. Gerstoft, P. M. Shearer, N. Harmon, J. Zhang, Global P, PP, and PKP wave microseisms observed from distant storms. *Geophys. Res. Lett.* **35**, L23306 (2008).
[doi:10.1029/2008GL036111](https://doi.org/10.1029/2008GL036111)
25. M. Landès, F. Hubans, N. M. Shapiro, A. Paul, M. Campillo, Origin of deep ocean microseisms by using teleseismic body waves. *J. Geophys. Res.* **115**, B05302 (2010).
[doi:10.1029/2009JB006918](https://doi.org/10.1029/2009JB006918)
26. P. Gouédard *et al.*, Cross-correlation of random fields: Mathematical approach and applications. *Geophys. Prospect.* **56**, 375 (2008). [doi:10.1111/j.1365-2478.2007.00684.x](https://doi.org/10.1111/j.1365-2478.2007.00684.x)
27. K. Wapenaar, E. Slob, R. Snieder, A. Curtis, Tutorial on seismic interferometry: Part 2—Underlying theory and new advances. *Geophysics* **75**, 75A211 (2010).
[doi:10.1190/1.3463440](https://doi.org/10.1190/1.3463440)
28. E. Kozlovskaya, M. Poutanen, POLENET/LAPNET Working Group, POLENET/LAPNET—a multidisciplinary geophysical experiment in northern Fennoscandia during IPY 2007-2008. *Eos* **87** (fall meet. suppl.), abstract S41A-1311 (2006).
29. T. Janik, E. Kozlovskaya, J. Yliniemi, Crust-mantle boundary in the central Fennoscandian shield: Constraints from wide-angle *P*- and *S*-wave velocity models and new results of reflection profiling in Finland. *J. Geophys. Res.* **112**, B04302 (2007).
[doi:10.1029/2006JB004681](https://doi.org/10.1029/2006JB004681)
30. P. Poli, M. Campillo, H. A. Pedersen, “Seismic noise tomography in regions with small velocity contrasts and strong noise directivity: Application to the northern Baltic Shield”; available at <http://hal.archives-ouvertes.fr/hal-00721895>.
31. B. L. N. Kennett, E. R. Engdahl, R. Buland, Constraints on seismic velocities in the Earth from travel times. *Geophys. J. Int.* **122**, 108 (1995). [doi:10.1111/j.1365-246X.1995.tb03540.x](https://doi.org/10.1111/j.1365-246X.1995.tb03540.x)
32. A. Alinaghi, G. Bock, R. Kind, W. Hanka, K. Wylegalla, TOR, SVEKALAPKO, Working Groups, Receiver function analysis of the crust and upper mantle from the North German

- Basin to the Archean Baltic Shield. *Geophys. J. Int.* **155**, 641 (2003). [doi:10.1046/j.1365-246X.2003.02075.x](https://doi.org/10.1046/j.1365-246X.2003.02075.x)
33. E. Ohtani, T. Sakai, Recent advances in the study of mantle phase transitions. *Phys. Earth Planet. Inter.* **170**, 240 (2008). [doi:10.1016/j.pepi.2008.07.024](https://doi.org/10.1016/j.pepi.2008.07.024)
34. L. Stixrude, C. Lithgow-Bertelloni, Thermodynamics of mantle minerals—II. Phase equilibria. *Geophys. J. Int.* **184**, 1180 (2011). [doi:10.1111/j.1365-246X.2010.04890.x](https://doi.org/10.1111/j.1365-246X.2010.04890.x)
35. T. Melbourne, D. Helmberger, Fine structure of the 410-km discontinuity. *J. Geophys. Res.* **103**, 10091 (1998). [doi:10.1029/98JB00164](https://doi.org/10.1029/98JB00164)
36. J. Lawrence, P. Shearer, Constraining seismic velocity and density for the mantle transition zone with reflected and transmitted waveform. *Geochem. Geophys. Geosyst.* **7**, Q10012 (2006). [doi:10.1029/2006GC001339](https://doi.org/10.1029/2006GC001339)
37. M. Bouchon, A simple method to calculate Green's functions for elastic layered media. *Bull. Seismol. Soc. Am.* **71**, 959 (1981).